J. Phys.: Condens. Matter **20** (2008) 395202 (11pp) doi:10.1088/0953-8984/20/39/395202

Dissecting quantum pathways in two-dimensional correlation spectroscopy of semiconductors

Lijun Yang and Shaul Mukamel

Chemistry Department, University of California, Irvine, CA 92697-2025, USA

E-mail: smukamel@uci.edu

Received 10 April 2008, in final form 3 July 2008
Published 1 September 2008
Online at stacks.iop.org/JPhysCM/20/395202

Abstract

We propose to employ multi-color narrow-bandwidth pulses to dissect the quantum pathways in two-dimensional correlation spectroscopy (2DCS) optical signals generated along the phase-matching directions $\mathbf{k_I} = -\mathbf{k}_1 + \mathbf{k}_2 + \mathbf{k}_3$ (photon echo) and $\mathbf{k_{III}} = \mathbf{k}_1 + \mathbf{k}_2 - \mathbf{k}_3$ (double quantum coherence). Simulations demonstrate how the resolution of 2DCS signals in GaAs quantum wells may be enhanced by spectrally selecting desired Liouville-space pathways. Pulse-shaping techniques may be used to further enhance the resolution.

(Some figures in this article are in colour only in the electronic version)

1. Introduction

Interference among different quantum pathways is one of the most fundamental and fascinating aspects of quantum mechanics. However, it complicates the analysis of the nonlinear optical response of semiconductors in terms of many-body interactions [1–14]. Two-dimensional correlation spectroscopy (2DCS) techniques [15–20], the femtosecond analogs of multi-dimensional NMR [21], spread the congested one-dimensional four-wave mixing (1D FWM) signals along two frequency axes. 2DCS allows us to separate some quantum pathways and combine the information to enhance the resolution [22]. However, this separation is not always complete. For example, for the double-quantum-coherence ($\mathbf{S_{III}}$) technique [23], in GaAs quantum wells (SQWs) within the rotating wave approximation (RWA), there are six pathways involving heavy-hole (HH) excitons and pure HH two-excitons, and six pathways involving LH excitons and pure LH two-excitons. If quantum interference among HH and LH excitons are included, then an extra 24 pathways arising from mixed two-excitons will be added.

In this paper we explore ways for controlling and minimizing these interferences. We first show how to isolate quantum pathways in the $S_{\mathbf{I}}$ (photon echo) signal generated along the phase-matching direction, $\mathbf{k_I} = -\mathbf{k}_1 + \mathbf{k}_2 + \mathbf{k}_3$, by employing narrow-bandwidth pulses. Within the RWA, there are three types of quantum (Liouville-space) pathways [24]. These are known as ground-state bleaching (GSB), excited-state emission (ESE) and excited-state absorption (ESA). Narrow-bandwidth excitations can select desired pathways. We then use the same approach to enhance the $S_{\mathbf{III}}$ signals along the phase-matching direction $\mathbf{k_{III}} = \mathbf{k}_1 + \mathbf{k}_2 - \mathbf{k}_3$. In a previous study [23], we proposed to use different polarization configurations of the optical pulses for probing various two-exciton correlations. Pure HH or LH (but not mixed) two-excitons are resolved. Here we show that mixed two-excitons can be selected and resolved. We further propose to employ pulse-shaping to suppress undesired signals.

2. Excitons and two-excitons in semiconductor quantum wells

The optical spectrum of GaAs SQWs connects a $J = \frac{3}{2}$ valence band and a $J = \frac{1}{2}$ conduction band (the $J = \frac{1}{2}$ valence band is usually neglected due to off-resonance). The conduction band can thus be accurately represented by two conduction orbitals $J_z = \pm\frac{1}{2}$ and four valence orbitals, $J_z = \pm\frac{3}{2}$ (HH) and $J_z = \pm\frac{1}{2}$ (LH) states [25, 26]. The dipole selection rules are presented in figure 1. The allowed transitions are denoted by R and L arrows, representing right and left circularly polarized photons, respectively.

The transition from $J_z = -\frac{3}{2}$ to $-\frac{1}{2}$ induced by an R photon forms an HH exciton denoted by $(-\frac{3}{2}, -\frac{1}{2})$. The other

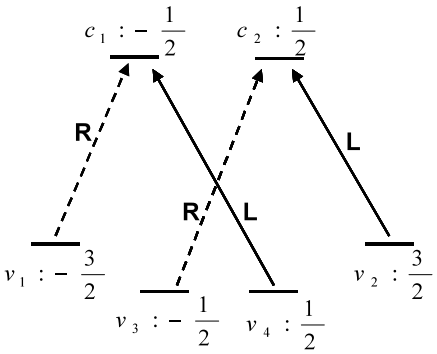

Figure 1. Spin orbital and selection rules for a single site of the quantum well model.

type of HH exciton $(\frac{3}{2}, \frac{1}{2})$ can be induced by an L photon. These two types of HH excitons degenerate in energy but have opposite spins. Similarly two types of LH excitons $(-\frac{1}{2}, \frac{1}{2})$ and $(\frac{1}{2}, -\frac{1}{2})$ can be generated by R and L photons, respectively. Two HH excitons can form pure HH two-excitons, denoted hereafter by $f_{\rm H}$, either bound or unbound, depending on whether the two HH single excitons are with opposite or same spins. Pure LH two-excitons ($f_{\rm L}$) can be formed by two single LH excitons. A single HH exciton and an LH exciton can also form a mixed two-exciton (denoted by $f_{\rm M}$). Only HH excitons and pure HH bound two-excitons have been well understood in the past. So far there are no experimental reports on the pure LH two-excitons due to their weak strength. The study of mixed two-excitons [27, 28] might be even more complicated because different quantum wells might have different dominance from either holes or electrons. So it is not straightforward to determine whether bound or unbound mixed two-excitons are generated because this might be related to specific systems.

3. Dissecting photon-echo 2DCS signals with narrow-bandwidth pulses

3.1. Feynman diagrams

2DCS employs four femtosecond laser pulses. Three time delays t_1, t_2 and t_3 are controlled between the chronologically ordered pulses $\mathbf{k}_1$, $\mathbf{k}_2$ and $\mathbf{k}_3$ and the last (heterodyne) pulse, $\mathbf{k}_s$. In this section, we focus on the photon-echo signal $S_{\mathbf{I}}(\Omega_3, t_2, \Omega_1)$ projected into the 2D plane (Ω_3, Ω_1), where Ω_3 and Ω_1 are, respectively, the Fourier frequencies conjugate to the time delays t_3 and t_1 [18]. We first present the Feynman diagrams [24] and the corresponding schematic 2DCS. The diagrams shown in figure 2 are generated from the three basic diagrams of the $S_{\mathbf{I}}$ signal by including all contributions of HH ($e_{\rm H}$) and LH ($e_{\rm L}$) exciton transitions [18]. The diagrams are grouped accordingly.

3.2. Schematic photon-echo signals in the projection (Ω_3, Ω_1) plane

The photon-echo signal $\mathbf{S}_{\mathbf{I}}(\Omega_3, t_2, \Omega_1)$ expected from the diagrams of figure 2 is schematically shown in figure 3. The contributions of each diagram to the signal are represented by the various symbols given at the bottom. In ESA diagrams, open circles describe the contributions from bare two-excitons (no energy shifts) whose contributions vary for $f_{\rm H}$, $f_{\rm L}$ and $f_{\rm M}$. We denote these by an open circle. Solid (open) symbols denote redshifted (blueshifted) two-excitons. Panels (i), (ii) and (iii) represent GSB, ESE and ESA contributions and panel (s) is their sum. 2DCS signals can be very complicated. Along the diagonal lines, we have GSB signals and populations of excitons. For cross peaks, we may have GSB signals, coherence peaks and also exciton transport. Narrow-bandwidth excitations can select specific pathways.

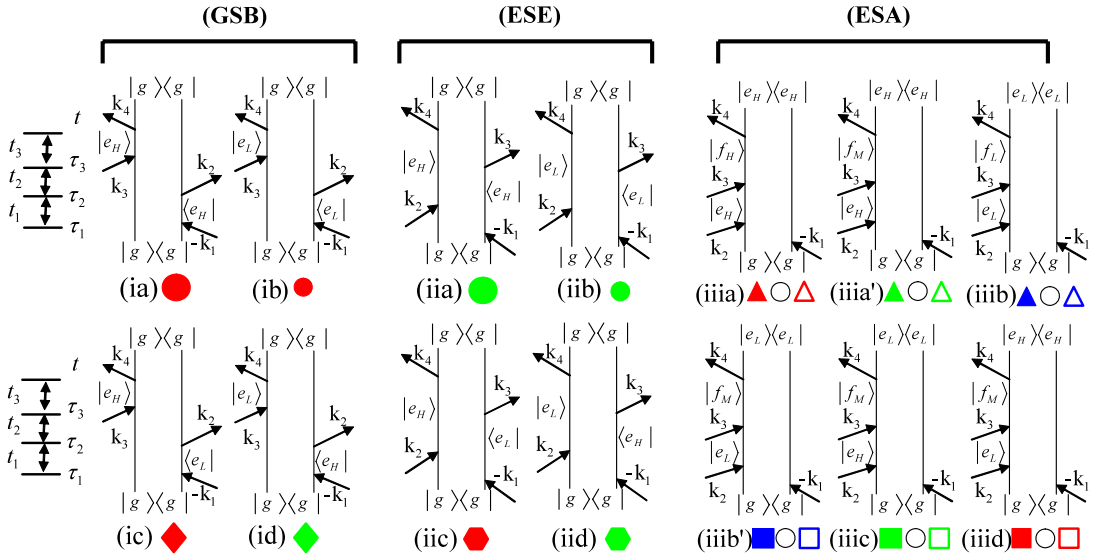

Figure 2. Feynman diagrams for the $S_{\mathbf{I}}$ technique. $e_{\rm H}$ and $e_{\rm L}$ denote, respectively, HH and LH excitons from the single-exciton manifold e. $f_{\rm H}$, $f_{\rm L}$ and $f_{\rm M}$ are from the two-exciton manifold f and denote, respectively, pure HH, pure LH and mixed two-excitons. g is the ground state.

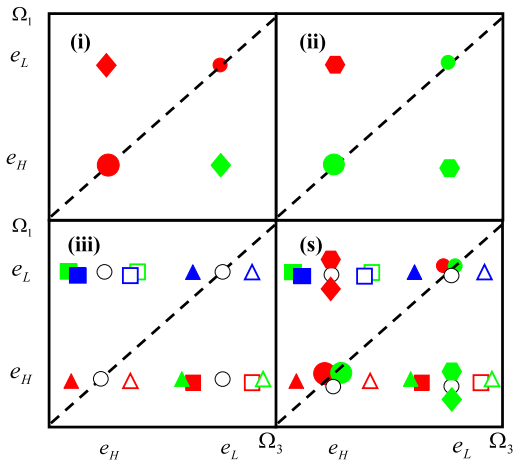

Figure 3. The $\mathbf{S_I}(\Omega_3, t_2, \Omega_1)$ signal derived from figure 2. (i) Diagrams (ia), (ib), (ic) and (id). (ii) Diagrams (iia), (iib), (iic) and (iid). (iii) Diagrams (iiia) to (iiid). (s) Total spectrum. Overlapping symbols are displaced for clarity.

3.3. Separation of excited-state emission

In [29], we showed that the ESE (the dominant Raman coherence between HH and LH excitons) contributions may not be isolated in the common $\mathbf{S_I}(\Omega_3, t_2, \Omega_1)$ projection but can be isolated with the $\mathbf{S_I}(\Omega_3, \Omega_2, t_1)$ projection. Here we demonstrate that, with narrow-bandwidth excitations, it is easy to isolate the Raman coherence in the $\mathbf{S_I}(\Omega_3, t_2, \Omega_1)$ projection. We first employ a pulse sequence (LH, HH, LH), where the first, second and third pulses can, respectively, excite only LH, HH and LH excitons due to their different colors and narrow spectral width. This pulse sequence selects only pathways (iic) and (iiic) in figure 2 and the corresponding schematic 2DCS is shown in figure 4 (bottom left). If we choose a different pulse sequence (HH, LH, HH), then the other two pathways (iid) and (iiid) are selected. The corresponding schematic 2DCS is shown in figure 4 (bottom right). Thus with these two pulse sequences, the ESE contributions ((iic) and (iid)) no longer overlap with the other dominant contribution from GSB pathways ((ic) and (id)) in photon-echo signals.

We next present numerical simulations based on a multi-band 1D tight-binding Hamiltonian [30–32] for a GaAs quantum well. The Heisenberg equations of motion derived from this Hamiltonian are closed by the dynamics-controlled truncation scheme [33, 4]. This 1D tight-binding model with simplified Coulomb interactions can include HH and LH excitons and their continuum states in a tractable way and qualitatively account for various features of 1D four-wave-mixing [32] and 2DCS signals [19, 23, 22]. We employ the same semiconductor quantum well parameters as in [23] which gives an LH–HH splitting of 3.8 meV and a binding energy of 1.2 meV for pure HH two-excitons. The optical fields are

$$\mathbf{E}(\mathbf{r}, t) = \sum_{\alpha=1}^{3} \left[\mathbf{E}_\alpha(\mathbf{r}, t) + \mathbf{E}_\alpha^*(\mathbf{r}, t)\right]$$
$$= \sum_{\alpha=1}^{3} \left[\mathbf{e}_\alpha \mathcal{E}_\alpha^+(t - t_\alpha)\, \mathrm{e}^{\mathrm{i}(\mathbf{k}_\alpha \cdot \mathbf{r} - \omega_\alpha t)} + \mathbf{e}_\alpha \mathcal{E}_\alpha^-(t - t_\alpha) \times \mathrm{e}^{-\mathrm{i}(\mathbf{k}_\alpha \cdot \mathbf{r} - \omega_\alpha t)}\right]. \quad (1)$$

Here $\mathcal{E}_\alpha^+$ ($\mathcal{E}_\alpha^- = (\mathcal{E}_\alpha^+)^*$) is the envelope of the positive-(negative)-frequency component of the αth pulse ($\alpha = 1, 2, 3, 4$) centered at t_α, with carrier frequency ω_α,

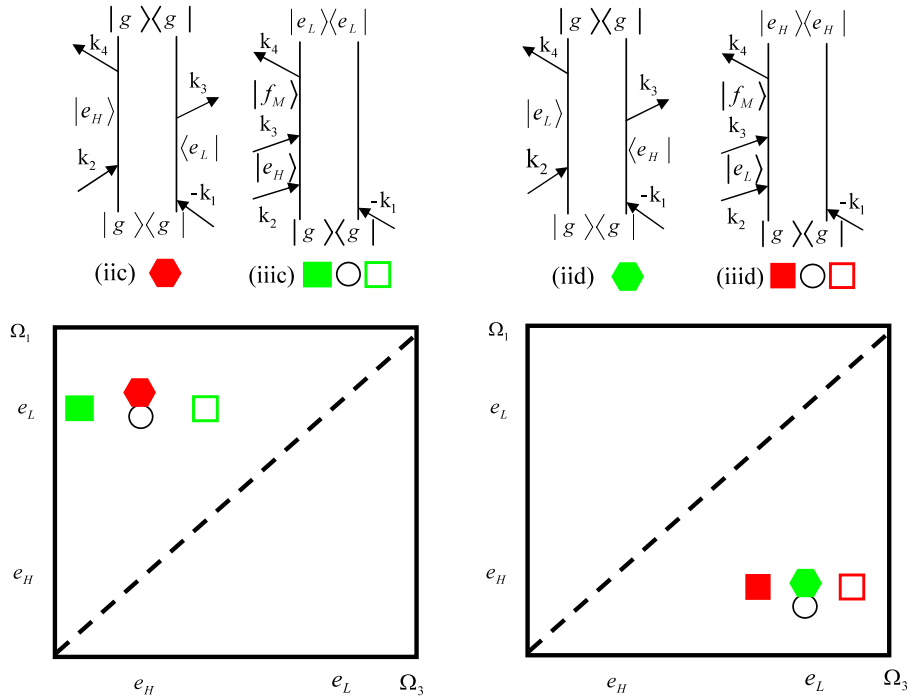

Figure 4. Selected Raman coherence pathways and the corresponding schematic 2DCS with: (left) a pulse sequence that excites only LH, HH and LH excitons, respectively; (right) a pulse sequence that excites only HH, LH and HH excitons, respectively. Overlapping symbols are displaced for clarity.

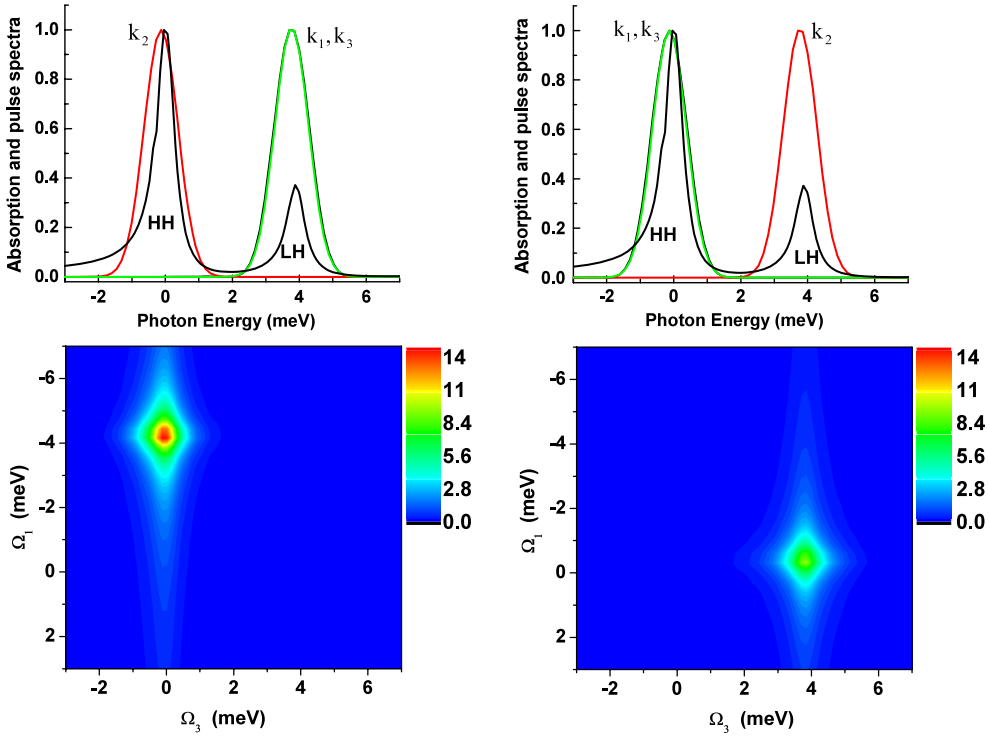

Figure 5. Left column (top) linear absorption and the spectra of an (LH, HH, LH) pulse sequence. (Bottom) 2DCS obtained with narrow-bandwidth pulses on top. Right column: the same as the left column except that an (HH, LH, HH) pulse sequence is employed. The origin for 2D spectra is at ($e_{\rm H}$, $e_{\rm H}$). Both t_2 and the initial value of t_1 take a value of 1.5 ps.

polarization unit vector $\mathbf{e}_\alpha$ and wavevector $\mathbf{k}_\alpha$. We assume Gaussian envelopes for all pulses:

$$\mathcal{E}_\alpha^{\pm}(t-t_\alpha) = \exp\left[-(t-t_\alpha)^2/\delta_\alpha^2\right]. \qquad (2)$$

Figure 5 shows simulated 2DCS signals using the same pulse sequences as in figure 4. We obtain the expected cross peaks as schematically shown in figure 4. Here we find that ESE signals (or the Raman coherence [29]) can be isolated in the 2D plane (Ω_3, Ω_1) with narrow-bandwidth pulses. However, this is impossible with broad-bandwidth pulses [29].

3.4. Separation of ground-state bleaching

With broad-bandwidth excitations, the GSB contributions may not be resolved in any 2D projection. In the $\mathbf{S_I}(\Omega_3, t_2, \Omega_1)$ projection shown in figure 3(s), (ic) (GSB) and (iic) (ESE) are both dominant and completely overlap with each other. The same is true for (id) (GSB) and (iid) (ESE) pathways. In the $\mathbf{S_I}(\Omega_3, \Omega_2, t_1)$ projection, the GSB pathways cannot be resolved either [29]. We next show that the GSB can be isolated with narrow-bandwidth excitations in the $\mathbf{S_I}(\Omega_3, t_2, \Omega_1)$ projection. Using (LH, LH, HH) and (HH, HH LH) pulse sequences, as described in figure 6, the cross peaks in the simulated signals shown in figure 7 represent pure GSB contributions.

We note that the ESA contributions always couple with either ESE or GSB and may not be separated. For example, in figure 4, diagram (iic) (ESE) is always coupled with (iiic) (ESA). In figure 6, we always have diagram (ic) (GSB) and (iiib′) (ESA) coupled together. However, in GaAs, the ESA contributions are usually very small as compared to the other two pathways.

4. Dissecting double-quantum-coherence (2DCS) signals with narrow-bandwidth excitations

4.1. Feynman diagrams

We now turn to the $\mathbf{k_{III}} = \mathbf{k}_1 + \mathbf{k}_2 - \mathbf{k}_3$ signal (adopting the notation of [23].), $S_{\rm III}(\Omega_3, \Omega_2, t_1)$. This technique has been shown to be particularly sensitive to two-exciton correlations in quantum wells [22, 23, 34], photosynthetic complexes [35] and in vibrational excitons [36]. The two basic pathways that contribute to the signal within the RWA are represented by the two basic double-sided Feynman diagrams shown at the bottom of figure 8.

These result in the 12 pathways shown in figure 9 if we enumerate e and f as ($e_{\rm H}$, $e_{\rm L}$) and ($f_{\rm H}$, $f_{\rm L}$, $f_{\rm M}$), respectively. These are separated into three groups (A), (B) and (C). The expected 2D spectrum is schematically shown in figure 10.

To select the desired quantum pathways, we employ spectrally narrow pulses. Group (A) is eliminated by using a spectrally narrow first pulse $\mathbf{k}_1$ that only excites HH but not LH excitons. If the second pulse is spectrally narrow as well, and tuned to the LH excitons, then group (B) is eliminated and only four quantum pathways (group (C)) survive. Finally, assuming a spectrally narrow third pulse $\mathbf{k}_3$ that only excites HH excitons, we can further eliminate pathways (viiia′) and

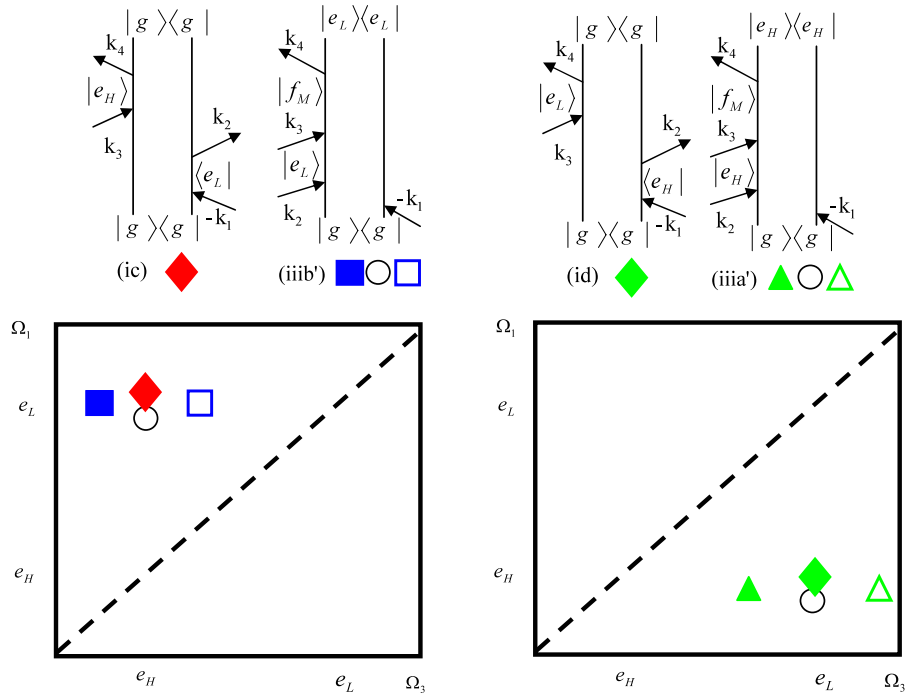

Figure 6. Selected GSB pathways and the corresponding schematic 2DCS with: (left) a pulse sequence that excites only LH, LH and HH excitons, respectively; (right) a pulse sequence that excites only HH, HH and LH excitons, respectively. Overlapping symbols are displaced for clarity.

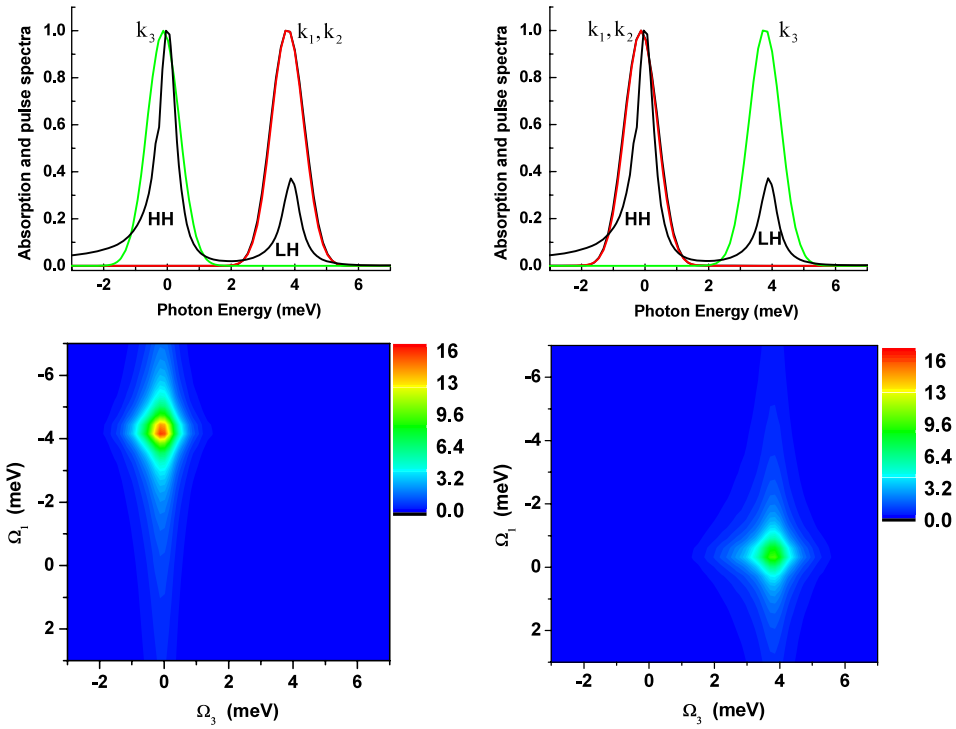

Figure 7. Simulated 2DCS for GSB pathways isolation. (Left) A pulse sequence (LH, LH, HH) where the first, second and third pulses only excite LH, LH and HH excitons, respectively (top), and the corresponding 2DCS signal (bottom); (right) a pulse sequence (HH, HH, LH) where the first, second and third pulses only excite HH, HH and LH excitons, respectively (top), and the corresponding 2DCS signal (bottom). The origin for 2D spectra is at (e_{H}, e_{H}). Both t_2 and the initial value of t_1 take a value of 1.5 ps.

(viid) from group (C) and we are left with the two pathways shown in figure 11 (top). The schematic 2D spectrum is given at the bottom.

Thus, by selectively exciting either HH or LH excitons, we can reduce the complicated 2D spectrum (figure 10) with the 12 pathways of figure 9 to the spectrum shown in

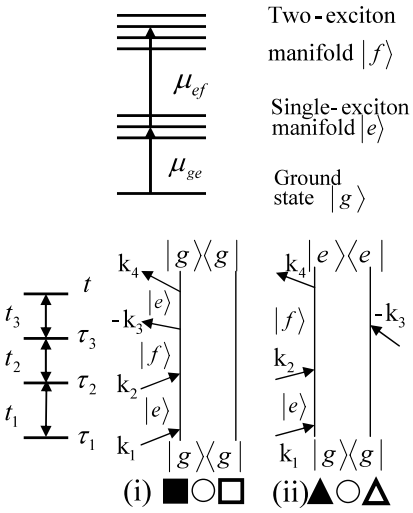

Figure 8. Exciton level scheme and Feynman diagrams for the S_{III} technique. The symbols at the bottom indicate the expected peaks in the 2D spectrum.

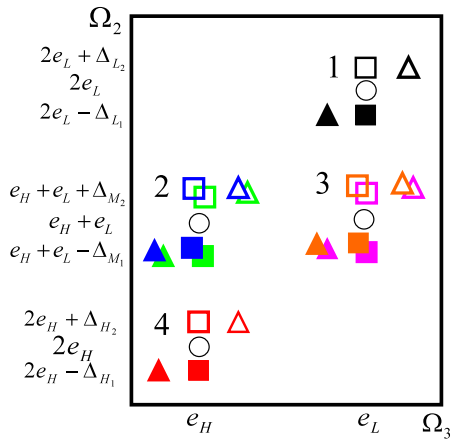

Figure 10. Schematic 2D S_{III} signals. Partially overlapped symbols in all panels occupy the same position but are displaced for clarity.

figure 11 (bottom). The two pathways of figure 11 (top) provide the correlation energies of mixed two-excitons. The solid (open) green symbols give, respectively, the binding and scattering energies of mixed two-excitons.

4.2. Simulations of multi-color 2DCS with double-quantum-coherence

To demonstrate the advantage of signal dissection by narrow-bandwidth pulses, we first present in figure 12(A) the absorption spectrum and pulse power spectra used in [23] which span both HH and LH excitons but not the continuum states. The pulse polarization configuration is XRLR, where the indices are chronologically ordered from right to left, i.e. $\mathbf{k_1}$ is R, right circularly polarized; $\mathbf{k_2}$ is L, left circularly polarized; $\mathbf{k_3}$ is R, right circularly polarized; and the heterodyne pulse $\mathbf{k_s}$ is X, linearly polarized in the X direction. This pulse sequence resolves the binding energies of pure HH and LH two-excitons, as respectively given by peaks (m, n) and (c, d) in figure 12(C) [23]. However, the binding energy of mixed two-excitons is not resolved because, apart from the peaks (m, n) induced by HH two-excitons, there are no peaks below either peak (e) or (f)[1]. This is due to two reasons. First, when the quantum well is excited by broadband pulses, all 36 pathways interfere and the information from mixed two-excitons is obscured by other stronger signals. Second, for the XRLR polarization configuration, the time-dependent Hartree–Fock (TDHF) contribution from mixed two-excitons (peaks (e) and (f)) is dominant [23] which complicates the probing of the binding energy of mixed two-excitons that goes beyond TDHF.

With the same broad-bandwidth pulses but different polarization configuration (XRRR) (figure 12(B)), we can eliminate the TDHF contribution from mixed two-excitons and

[1] There are indeed some features below peak (e). However, they are artificial features and change when calculated with different basis sets, as shown in [23].

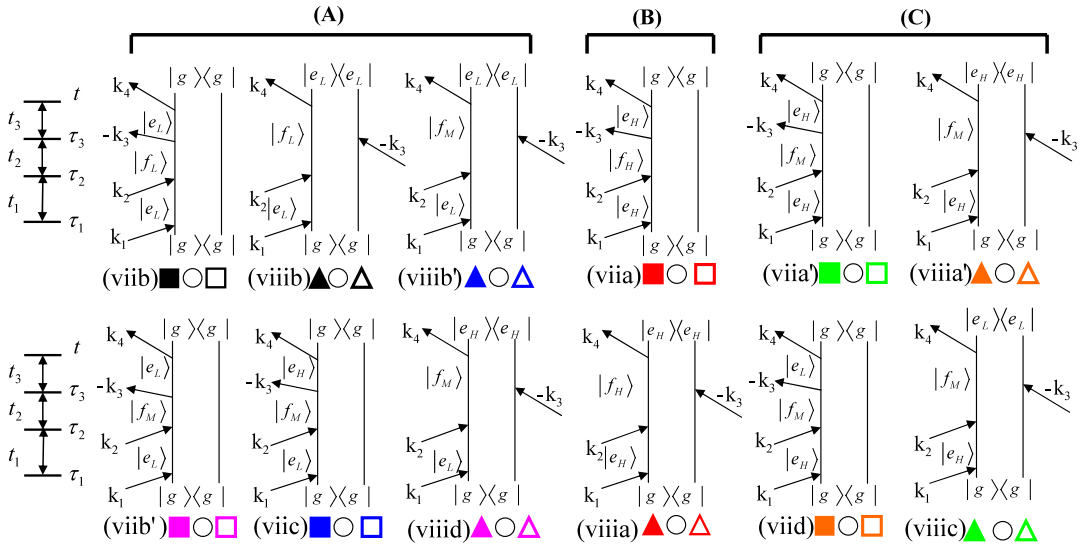

Figure 9. Complete Feynman diagrams for S_{III} signals of an LH and HH exciton coupling system.

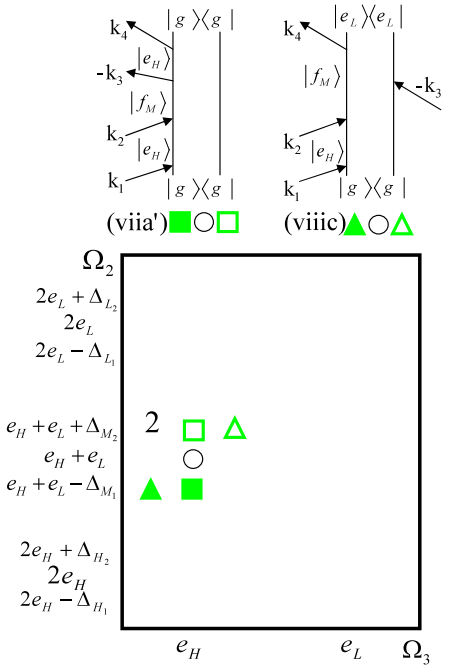

Figure 11. Top: Feynman diagrams for S_{III} signals of an LH and HH coupled system. The first, second and third pulses only excite HH, LH and LH excitons, respectively. Bottom: the expected schematic 2D spectrum.

have only the higher-order correlation effects left. However, we still could not infer either the red- or blueshifted scattering energy among mixed two-excitons, as shown in figure 12(D).

Let us probe the correlation energies of mixed two-excitons [27, 28] with narrow-bandwidth pulses. The absorption spectrum and the power spectra ($|\mathcal{E}_\alpha(\omega)|^2$) of the various pulses used in our simulations are shown in figure 13. The corresponding 2D spectra are respectively given in figure 14. We first focus on the binding energy of mixed two-excitons and still employ the XRLR polarization configuration. The pulses can excite either HH or LH excitons, but not both. The first, second and third pulses are spectrally narrow and can only excite HH, LH or LH excitons, respectively. The power spectra of the three pulses are shown in figure 13(A) and the resulting 2D spectrum which depends on two pathways (figure 11 top) is shown in figure 14(A). All 2D spectra in figure 14 are calculated with 20 sites with periodic boundary conditions [32]. Figure 13(A) selects mixed two-excitons in region 2 of figure 10. Thus the signal in figure 14(A) is solely attributed to mixed two-excitons and their binding energy can be clearly seen from the Ω_2 value of peak (b), relative to the bare mixed two-excitons with $\Omega_2 = e_{\mathrm{H}} + e_{\mathrm{L}} \approx 4$ meV. The Ω_2 value of peak (b) can be read precisely from the white line connecting the ridges of involved contour lines, even though peak (b) is not resolved along Ω_3. For the specific parameters [23] used in our simulations, the binding energy of mixed two-excitons is around 2.3 meV. However, this number expects to vary for different semiconductor materials and various quantum well widths.

The same technique can be used to resolve the even weaker blueshifted scattering energy among mixed two-excitons. In figure 13(B), we employ the same XRRR

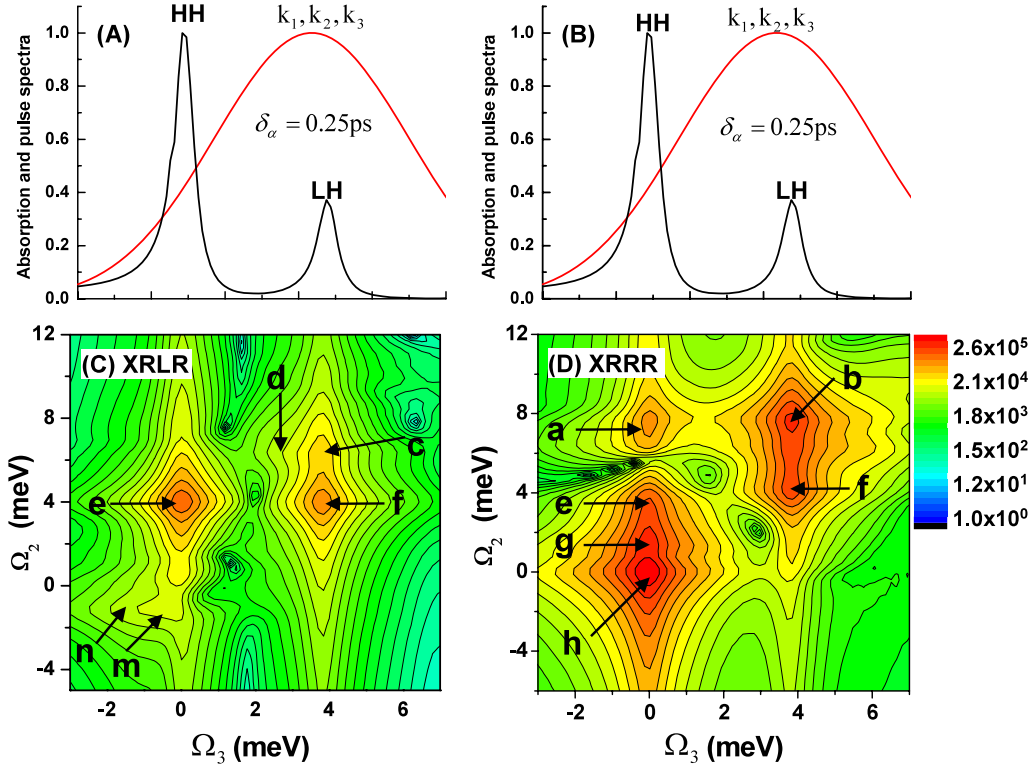

Figure 12. (Top) Linear absorption of a GaAs quantum well and the pulse power spectra used in the simulations. (Bottom) The corresponding 2D spectra calculated with $t_1 = 0.3$ ps for panel (C) and $t_1 = 0.15$ ps for panel (D). The origin for 2D spectra is at (e_{H}, $2e_{\mathrm{H}}$).

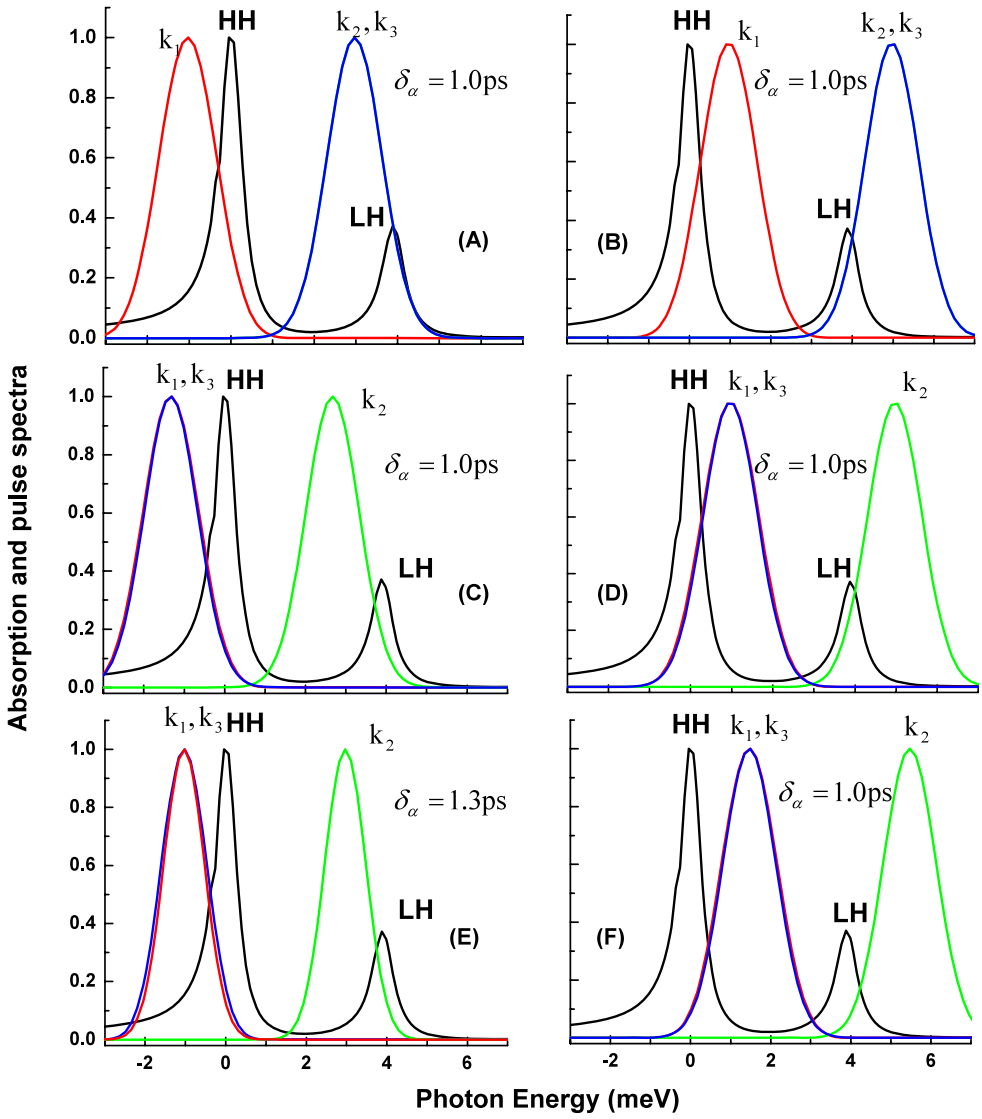

Figure 13. Linear absorption of a GaAs quantum well and the pulse power spectra used in the various simulations.

polarization configuration but with multi-color narrow-bandwidth pulses. The 2D spectrum (figure 14(B)) clearly reveals the blueshifted scattering energies of mixed two-excitons by the Ω_2 value of peak (b), relative to the bare mixed two-excitons peak (a).

We next turn from region 2 to region 3 in figure 10 in order to probe mixed two-excitons. Using the Feynman diagrams, we expect to obtain the same results from this region. To select region 3, we detune the three pulses as shown in figures 13(C) and (D). The corresponding 2D spectra are shown in figures 14(C) and (D). Regions 1, 2 and 4 are now eliminated. In figure 14(C), peak (b) or the Ω_2 value of the white line connecting the ridges of contour lines gives the binding energy of bound mixed two-excitons. In figure 14(D), peak (b) or the Ω_2 value of the white line gives the scattering energy of unbound mixed two-excitons. In both figures, peak (a) corresponds to the TDHF contribution. The correlation energies in figures 14(C) and (D) obtained from region 3 are the same as from region 2 (figures 14(A) and (B)).

Figures 14(C) and (D) used circularly polarized pulses to eliminate the corresponding TDHF contribution. We can also resolve correlation energies of mixed two-excitons by employing collinearly polarized pulses. Figures 14(E) and (F) are obtained with XXXX polarization configuration but with different detunings of pulse center frequency (figures 13(E) and (F)) and slightly different pulse bandwidths. In this case, we cannot suppress the TDHF contribution of a certain type of two-excitons to highlight the beyond-TDHF contribution [23]. However, we can still tune the carrier frequencies to control the relative strength of the TDHF contribution compared to higher level contributions. From figures 14(E) and (F), we can clearly see the binding and scattering energies of mixed two-excitons.

4.3. Discussion

In figure 11 we selected half of the pathways in region 2 of figure 10. We eliminated the influence of pure HH (or LH) two-excitons in the probing of mixed two-excitons and the possible interferences among pathways arising from mixed

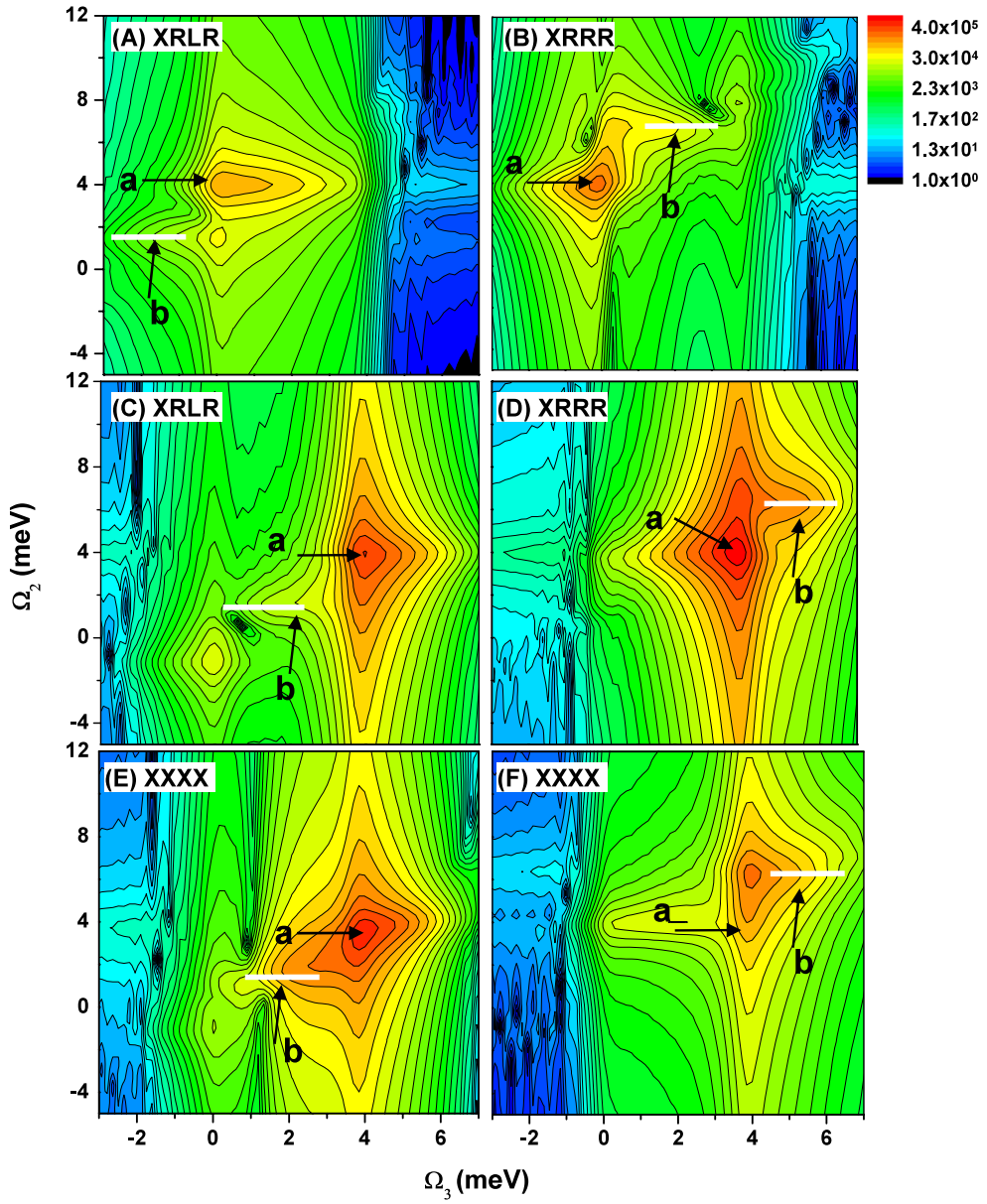

Figure 14. Simulated $S_{\mathrm{III}}(\Omega_3, \Omega_2, t_1)$ spectra ($t_1 = 1.2$ ps) for the pulse configurations shown in figure 13. The origin of the 2D spectra is at $(e_{\mathrm{H}}, 2e_{\mathrm{H}})$.

two-excitons. In figure 11 (bottom), we retain the signals coming from two mixed two-exciton pathways and turn off the other two (comparing the signals in region 2 of figure 10 where both blue and green symbols coexist and the signals at the bottom of figure 11 which only show green symbols). With this pulse sequence, we show by numerical calculations that multi-color 2DCS can improve the resolution to mixed two-excitons. Unlike the techniques based on polarized pulses [23] which depend specifically on the selection rules, the multi-color 2DCS technique can be applied to general molecular electron–hole systems. Finally, similar to selecting either region 2 (figures 14(A) and (B)) or 3 (figures 14(C)–(F)), we can also design pulse sequences that only show regions 1 or 4, which will yield high resolution of pure HH or LH two-excitons.

5. Suppressing undesired signals with pulse-shaping

Considering only HH excitons, the two pathways in $\mathbf{S}_{\mathrm{III}}$ contribute to the signal. Both pathways contain some contributions (e.g. those from bare two-excitons with twice the single-exciton energy) that can generally affect the resolution of two-exciton correlations. We cannot probe both the bound and unbound two-excitons in one shot but must observe them in different experiments [22].

To suppress the bare two-exciton contribution from the irreducible pathways, we can use the same color but shaped pulses [37, 38]. We employ shaped pulses with double peaked spectrum to the red and blue of HH excitons, given by equation (3). Such pulses have been generated by cutting out of the spectrum of a broadband Ti:sapphire laser pulse to

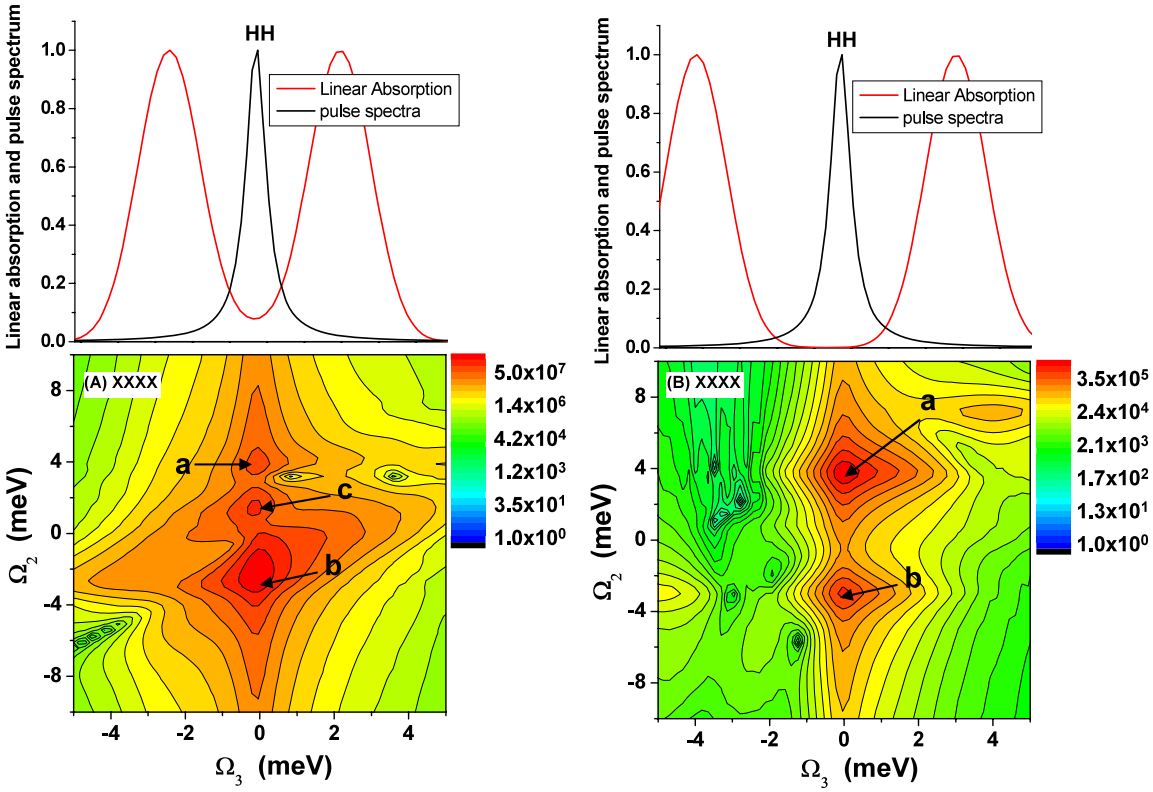

Figure 15. Left column (top): linear absorption and the pulse power spectrum corresponding to the 2D spectra below. The pulse spectrum has two peaks, centered at −2.35 meV and 2.25 meV, respectively. (Bottom) 2DCS obtained with spectrally shaped pulses on top. Right column: the same as the left column except that the two peaks of the pulse power spectrum are centered at −3.85 meV and 3.15 meV, respectively.

generate terahertz radiation [39]:

$$\mathcal{E}_\alpha^+(t-t_\alpha) = \exp\left[-(t-t_\alpha)^2/\left(\delta_\alpha^A\right)^2\right] e^{-i\omega_A t} + \exp\left[-(t-t_\alpha)^2/\left(\delta_\alpha^B\right)^2\right] e^{i\omega_B t}. \quad (3)$$

The pulses have the same carrier frequency, ω_α, and shape: two Gaussian peaks at ω_A and ω_B (top of figure 15), which are off resonant from the HH excitons at $\omega = 0$ meV. This pulse may be used to investigate the HH excitons using the same parameters of [31]. The exciton and two-exciton dephasing times are set, respectively, to $\tau_{ex} = 2$ ps and $\tau_{2ex} = 1$ ps. Because all pulses are detuned from the HH excitons, we expect the influence of bare two-excitons to be significantly suppressed. The 2D spectrum shown in the bottom left of figure 15 is calculated using pulses with the same two-peaked spectrum (top left). The red- and blueshifted correlation energies of mixed two-excitons are respectively given by peaks (b) and (a). Note that these correlation energies are observed simultaneously in a single 2D spectrum. In the right column of figure 15, we employed different two-peaked pulses with a larger splitting between ω_A and ω_B. As expected, we obtain the same correlation energies given by peaks (a) and (b). However, the bare two-exciton contributions are further suppressed due to the larger splitting of the two peaks in the pulse spectrum.

In conclusion, we proposed to employ multi-color narrow-bandwidth pulses to selectively detect specific pathways in photon-echo signals and electronic correlations of mixed two-excitons in double-quantum-coherence (2DCS) signals. The quantum pathways are controlled by designing multi-color narrow-bandwidth pulses and eliminating some undesirable pathways. This cancels some quantum interferences that usually prevent the observation of some weak features.

Acknowledgments

The support of the Chemical Sciences, Geosciences, and Biosciences Division, Office of Basic Energy Sciences, US Department of Energy is gratefully acknowledged.

References

[1] Haug H and Koch S W 2004 *Quantum Theory of the Optical and Electronic Properties of Semiconductors* 4th edn (Singapore: World Scientific)
[2] Shah J 1999 *Ultrafast Spectroscopy of Semiconductors and Semiconductor Nanostructures* 2nd enlarged edn (Berlin: Springer)
[3] Chemla D S and Shah J 2001 Many-body and correlation effects in semiconductors *Nature* **411** 549–57
[4] Axt V M and Mukamel S 1998 Nonlinear optics of semiconductor and molecular nanostructures; a common perspective *Rev. Mod. Phys.* **70** 145–74
[5] Rossi F and Kuhn T 2002 Theory of ultrafast phenomena in photoexcited semiconductors *Rev. Mod. Phys.* **74** 895–950

[6] Leo K, Wegener M, Shah J, Chemla D S, Göbel E O, Damen T C, Schmitt-Rink S and Schäfer S 1990 Effects of coherent polarization interactions on time-resolved degenerate four-wave mixing *Phys. Rev. Lett.* **65** 1340–3
[7] Lindberg M, Hu Y Z, Binder R and Koch S W 1994 $\chi^{(3)}$ formalism in optically excited semiconductors and its applications in four-wave-mixing spectroscopy *Phys. Rev.* B **50** 18060–72
[8] Leitenstorfer A, Lohner A, Elsaesser T, Haas S, Rossi F, Kuhn T, Klein W, Boehm G, Traenkle G and Weimann G 1994 Ultrafast coherent generation of hot electrons studied via band-to-acceptor luminescence in GaAs *Phys. Rev. Lett.* **73** 1687–90
[9] Kwong N H and Binder R 2000 Green's function approach to the dynamics-controlled truncation formalism: derivation of the $\chi^{(3)}$ equations of motion *Phys. Rev.* B **61** 8341–58
[10] Schäfer W, Kim D S, Shah J, Damen T C, Cunningham J E, Goossen J E, Pfeiffer L N and Köhler K 1996 Femtosecond coherent fields induced by many-particle correlations in transient four-wave mixing *Phys. Rev.* B **53** 16429–43
[11] Wang H, Ferrio K B, Steel D G, Hu Y Z, Binder R and Koch S W 1993 Transient nonlinear optical response from excitation induced dephasing in GaAs *Phys. Rev. Lett.* **71** 1261–4
[12] Östreich Th, Schönhammer K and Sham L J 1995 Exciton–exciton correlation in the nonlinear optical regime *Phys. Rev. Lett.* **74** 4698–701
[13] Bartels G, Axt V M, Victor K, Stahl A, Leisching P and Köhler K 1995 $\chi^{(5)}$ signature in the four-wave-mixing signal from a GaAs/$Al_{0.3}Ga_{0.7}$ As superlattice *Phys. Rev.* B **51** 11217–20
[14] Hawton M and Dignam M M 2003 Infinite-order excitonic Bloch equations for asymmetric nanostructures *Phys. Rev. Lett.* **91** 267402
[15] Mukamel S 2000 Multidimensional femtosecond correlation spectroscopies of electronic and vibrational excitations *Annu. Rev. Phys. Chem.* **51** 691–729
[16] Li X, Zhang T H, Borca C N and Cundiff S T 2006 Many-body interactions in semiconductors probed by optical two-dimensional Fourier transform spectroscopy *Phys. Rev. Lett.* **96** 57406
[17] Borca C N, Zhang T H, Li X and Cundiff S T 2005 Optical two-dimensional Fourier transform spectroscopy of semiconductors *Chem. Phys. Lett.* **416** 311–5
[18] Yang L, Schweigert I V, Cundiff S T and Mukamel S 2007 Two-dimensional optical spectroscopy of excitons in semiconductor quantum wells Liouville-space pathway analysis *Phys. Rev.* B **75** 125302
[19] Kuznetsova I, Thomas P, Meier T, Zhang T H, Li X, MirinR P and Cundiff S T 2007 Signatures of many-particle correlations in two-dimensional Fourier-transform spectra of semiconductor nanostructures *Solid State Commun.* **142** 154–8
[20] Langbein W and Patton B 2007 Transient coherent nonlinear spectroscopy of single quantum dots *J. Phys.: Condens. Matter* **19** 295203
[21] Ernst R R, Bodenhausen G and Wokaun A 1987 *Principles of Nuclear Magnetic Resonance in One and Two Dimensions* (Oxford: Clarendon)
[22] Yang L and Mukamel S 2008 Two-dimensional correlation spectroscopy of two-exciton resonances *Phys. Rev. Lett.* **100** 057402
[23] Yang L and Mukamel S 2008 Revealing exciton–exciton couplings in semiconductors using multidimensional four-wave mixing signals *Phys. Rev.* B **77** 075335
[24] Mukamel S 1995 *Principles of Nonlinear Optical Spectroscopy* Paperback edn (New York: Oxford University Press)
[25] Meier F and Zakharchenya B P 1984 *Optical Orientation, in Modern Problems in Condensed Matter Sciences* vol 8 (Amsterdam: North-Holland)
[26] Bott K, Heller O, Bennhardt D, Cundiff S T, Thomas P, Mayer E J, Smith G O, Eccleston R, Kuhl J and Ploog K 1993 Influence of exciton–exciton interactions on the coherent optical response in GaAs quantum wells *Phys. Rev.* B **48** 17418–26
[27] Wagner H P, Langbein W and Hvam J M 1999 Mixed biexcitons in single quantum wells *Phys. Rev.* B **59** 4584–7
[28] Meier T, Koch S W, Phillips M and Wang H 2000 Strong coupling of heavy- and light-hole excitons induced by many-body correlations *Phys. Rev.* B **62** 12605–8
[29] Yang L, Zhang T H, Cundiff S T and Mukamel S 2008 *J. Chem. Phys.* submitted
[30] Sieh C, Meier T, Jahnke F, Knorr A, Koch S W, Brick P, Hübner M, Ell C, Prineas J, Khitrova J and Gibbs H M 1999 Coulomb memory signatures in the excitonic optical Stark effect *Phys. Rev. Lett.* **82** 3112–5
[31] Weiser S, Meier T, Möbius J, Euteneuer A, Mayer E J, Stolz W, Hofmann M, Rühle W W, Thomas P and Koch S W 2000 Disorder-induced dephasing in semiconductors *Phys. Rev.* B **61** 13088–98
[32] Meier T, Thomas P and Koch S W 2007 *Coherent Semiconductor Optics: from Basic Concepts to Nanostructure Applications* (Berlin: Springer)
[33] Axt V M and Stahl A 1994 A dynamics-controlled truncation scheme for the hierarchy of density matrices in semiconductor optics *Z. Phys.* B **93** 195–204
[34] Mukamel S, Oszwaldowski R and Yang L 2007 *J. Chem. Phys.* **127** 221105
[35] Abramavicius D, Voronine D and Mukamel S 2007 *Proc. Natl Acad. Sci.* **105** 8525–30
[36] Abramavicius D and Mukamel S 2005 *Chem. Phys.* **318** 50–70
[37] Weiner A M 2000 Femtosecond pulse shaping using spatiallight modulators *Rev. Sci. Instrum.* **71** 1929–60
[38] Goswami D 2003 Optical pulse shaping approaches to coherent control *Phys. Rep.* **374** 385–481
[39] Rosam B, Leo K, Yang L and Dignam M M 2004 Terahertz generation by difference frequency mixing of excitonic Wannier–Stark ladder states in biased semiconductor superlattices *Appl. Phys. Lett.* **85** 4612–4